DNP NMR of biomolecular assemblies

Kristaps Jaudzems, Tatyana Polenova, Guido Pintacuda, Hartmut Oschkinat, Anne Lesage

DNP NMR of Biomolecular Assemblies

Kristaps Jaudzems,[(1)] Tatyana Polenova,[(2)] Guido Pintacuda,[(1)] Hartmut Oschkinat[(3)] and Anne Lesage[(1)]

(1) Centre de RMN à Très Hauts Champs, Institut des Sciences Analytiques (UMR 5280 - CNRS, ENS Lyon, UCB Lyon 1), Université de Lyon, 5 rue de la Doua, 69100 Villeurbanne, France

(2) Department of Chemistry and Biochemistry, University of Delaware, 163 The Green, DE 19716, USA

(3) Leibniz-Forschungsinstitut für Molekulare Pharmakologie im Forschungsverbund Berlin e.V. (FMP) Campus Berlin-Buch Robert-Roessle-Str. 10 13125 Berlin, Germany

Abstract: Dynamic Nuclear Polarization (DNP) is an effective approach to alleviate the inherently low sensitivity of solid-state NMR (ssNMR) under magic angle spinning (MAS) towards large-sized multi-domain complexes and assemblies. DNP relies on a polarization transfer at cryogenic temperatures from unpaired electrons to adjacent nuclei upon continuous microwave irradiation. This is usually made possible via the addition in the sample of a polarizing agent. The first pioneering experiments on biomolecular assemblies were reported in the early 2000s on bacteriophages and membrane proteins. Since then, DNP has experienced tremendous advances, with the development of extremely efficient polarizing agents or with the introduction of new microwaves sources, suitable for NMR experiments at very high magnetic fields (currently up to 900 MHz). After a brief introduction, several experimental aspects of DNP enhanced NMR spectroscopy applied to biomolecular assemblies are discussed. Recent demonstration experiments of the method on viral capsids, the type III and IV bacterial secretion systems, ribosome and membrane proteins are then described.

Keywords: Solid-state NMR; Dynamic Nuclear Polarization; Biological assemblies; Protein structure and dynamics; Magic Angle Spinning.

1. Introduction

High-resolution solid-state NMR (ssNMR) under magic angle spinning (MAS) has recently emerged as a powerful structural tool for studying structure and dynamics of non-crystalline macromolecular complexes. The inherently low sensitivity of this spectroscopy limits however its applicability, and as a result large-sized multi-domain complexes and assemblies still often remain inaccessible to site-specific structural studies.

In the last two decades, Dynamic Nuclear Polarization (DNP) has emerged as a key method to increase the sensitivity of MAS solid-state NMR spectroscopy. The first proofs of principle on biomolecular assemblies were reported in the early 2000s by Griffin and co-workers on bacteriophages and membrane proteins (Bajaj et al., 2003; Rosay et al., 2001; Rosay et al., 2003). Since then, thanks to great progress in instrumentation operating at higher and higher frequencies (Barnes et al., 2012; Ni et al., 2013) and to the introduction of tailor-designed polarizing agents (Sauvee et al., 2013; Sauvee et al., 2016; Song et al., 2006), DNP has established itself as a key tool for the investigation of a wide range of biological solids, from fibrils (Bayro et al., 2011; Debelouchina et al., 2010; Frederick et al., 2017; Potapov et al., 2015) to biomaterials (Geiger et al., 2016b; Jantschke et al., 2015; Ravera et al., 2015), membrane embedded proteins (Becker-Baldus et al., 2015), intrinsically

disordered proteins (Uluca et al, 2018) or cells (Frederick et al., 2015; Renault et al., 2012; Albert el al., 2018) to name but a few, thus gaining more and more importance in structural biology.

Several landmark review articles have already discussed the potential of DNP MAS NMR in this area (Akbey and Oschkinat, 2016; Su et al., 2015;). Throughout the present review, we will focus more specifically on recent advances on biomolecular assemblies. Experimental aspects of DNP enhanced NMR spectroscopy will first be discussed. The scope of the method will then be illustrated within the context of the structural investigation of viral capsids, the type III and IV bacterial secretion systems, ribosome and membrane proteins. Fibrillar assemblies are not included in this article.

2. Experimental aspects of DNP MAS NMR for biomolecular assemblies

2.1. Principle

DNP relies on a transfer of polarization between unpaired electron spins and surrounding nuclei. The samples are usually doped with stable radicals (the polarizing agents) and the unpaired electrons are saturated by continuous micro-wave (MW) irradiation. This is accomplished using gyrotrons that operate in the required frequency range (140–600 GHz) and produce high-power microwaves. The relaxation times of the unpaired electrons must be sufficiently long to allow saturation of the transitions, which is achieved by performing the experiments at low temperatures (usually ~100 K) using cryogenic MAS probes. Continuous wave DNP can proceed via several mechanisms that dictate the choice of the polarizing agent. Currently, the most efficient polarization transfer scheme for high-field MAS DNP experiments is the cross-effect mechanism, which requires a dipolar-coupled system of two electrons and a nucleus, and which is thus particularly effective with chemically stable organic biradicals (Can et al., 2015). This mechanism dominates when the resonance frequencies of the two electrons of the biradical are separated by the nuclear Larmor frequency. To date, the most successful biradicals for biomolecular studies are the water soluble binitroxides TOTAPOL (Song et al., 2006) and AMUPol (Sauvee et al., 2013). Like all nitroxides, they have an inhomogeneously broadened EPR line width that is comparable to the ^{1}H Larmor frequencies of contemporary NMR spectrometers (hundreds of MHz), allowing polarization transfer from the electrons to neighboring ^{1}H nuclei. The DNP-enhanced ^{1}H polarization is then transported in the sample by ^{1}H-^{1}H spin diffusion and subsequently transferred to heteronuclei via cross-polarization. The sensitivity enhancement by DNP, referred to as ε, can be measured as the ratio of signal intensities in NMR spectra acquired with and without microwave irradiation.

2.2. Water-soluble polarizing sources

TOTAPOL was the first popular water-soluble biradical polarizing agent and was shown to yield enhancements of up to ~80 at 400 MHz at 100 K. AMUPol was designed later to be more rigid and to possess longer electron relaxation times and stronger electron-electron couplings, improving by more than a factor of 3 the enhancement factors under identical conditions (typically 235 at 400 MHz, 128 at 600 MHz and 35 at 800 MHz for frozen bulk aqueous solutions). A direct comparison between the overall sensitivity gains obtained using TOTAPOL and AMUPol has been recently reported, confirming the overperformance of the latter (Mentink-Vigier et al., 2015). Only these two radicals have been used for the DNP studies of molecular assemblies discussed in this article (Table 1).

We note that several new biradicals, specifically designed for biomolecular DNP studies, have recently been introduced. Notable examples include new families of binitroxides like bcTol (Jagtap et al., 2016) or PyPolPEG2OH (Sauvee et al., 2016) as well as trityl-nitroxide biradicals TEMTriPols (Mathies et al., 2015). bcTol delivers similar sensitivity enhancements as AMUPol, but exhibits unparalleled solubility in water and glycerol/water mixtures as well as somewhat improved temperature dependence. PyPolPEG2OH is a

derivative of AMUPol that provides better anchoring in the glycerol/water matrix through additional hydrogen bonds resulting in longer T_{1e} and ca. 1.2 times higher enhancement factor. All binitroxides suffer from an unfavourable magnetic field dependence, as their EPR line width increases linearly with B_0, which in turn decreases the efficiency of the cross-effect mechanism (Maly et al., 2008). Conversely, TEMTriPols show unprecedented performance at high magnetic fields with a record ^{1}H NMR signal enhancement of 65 at 800 MHz and 100 K, almost a factor of two higher than AMUPol under similar experimental conditions.

The search for better-performing cross-effect DNP polarizing agents is still ongoing as the parameters of the current biradicals are far from optimal, and as the enhancements achieved today are still far from the theoretical maximum (658 for ^{1}H). Thus, it remains to be seen if any of the recently introduced or forthcoming biradicals will replace today's gold standard AMUPol in future biomolecular DNP studies. It should also be noted that in parallel, efforts are made to develop radicals for high-field DNP applications exploiting the Overhauser effect which scales favorably with the magnetic field (Can et al., 2014), instead of the cross-effect.

Obtaining a large enhancement requires that the radicals are well dispersed in the sample to avoid inter-radical interactions, which is conventionally achieved by using a glycerol/water or a DMSO/water glass-forming solvent (see the next paragraph). An alternative method, which also ensures a homogeneous dispersion of the radical, is "targeted DNP". In this approach, the radical is covalently attached either directly to the molecule of interest or to its binding partner using a linker (e.g. via cysteine mutagenesis and sulfhydryl chemistry). Nitroxide monoradicals as well as the biradicals TOTAPOL and AMUPol have been attached to peptides,(Vitzthum et al., 2011) to membrane proteins, (van der Cruijsen et al., 2015; Voinov et al., 2015; Wylie et al., 2015), to lipids (Fernandez-de-Alba et al., 2015; Smith et al., 2015) and to an interaction partner of the target protein (Rogawski et al., 2017; Viennet et al., 2016). In parallel, complexes of paramagnetic metal ions like Gd^{3+} and Mn^{2+} have been attached to proteins for site-selective DNP experiments (Kaushik et al, 2016). While the DNP enhancements provided by these approaches are generally comparable to those obtained by untargeted means, they offer the additional benefits of increased the filling factor removing the need of a glassy matrix, of exploiting a site-directed specificity in terms of enhancement and of using paramagnetic relaxation enhancement (PRE) effects from the radicals to obtain structural information. Notably, these methods have shown a great potential for studies of membrane proteins, where uniform dispersion of the radical in the membranes may otherwise be difficult. No targeted DNP studies have been reported so far on molecular assemblies.

2.3. Sample preparation

Multiple studies have investigated the impact of different sample preparation protocols, composition of the polarizing medium, protein and matrix deuteration levels and concentration of the polarizing agents on the DNP enhancement. Table 1 lists the experimental conditions used in most of the recent DNP-enhanced NMR studies of various molecular assemblies.

Insert Table 1 here.

A common way to perform DNP studies of proteins is to use frozen solutions (Siemer et al., 2012). Upon freezing, pure water forms ice crystals, which may spatially sequester the different sample components (protein, polarizing agent and water) in different domains, and lead to aggregation of the radical and poor enhancement. Therefore, most studies are performed in mixtures of water and glycerol, which are known to form a glass at low temperatures. A drawback of frozen solutions is that the filling factor and consequently the absolute sensitivity is relatively low as the vast majority of the sample volume is taken by the

solvent. To avoid this, the protein samples can be first precipitated by crystallization (Geiger et al., 2016a; van der Wel et al., 2006) or sedimentation (Ravera et al., 2014; Ravera et al., 2013), and then immersed in a solution containing a cryo-protectant before freezing. In favorable cases the samples can be measured in the absence of a glass forming agent. An early investigation on apoferritin by the group of Bertini (Ravera et al., 2013), for example, used sedimented proteins (*via* ultracentrifugation) that were very concentrated and obtained an enhancement of $\varepsilon > 40$ at 212 MHz and 90 K. This was achieved without adding glycerol as glass-forming agent, suggesting the formation of a glass-like state when solutions of such a high concentration are frozen. A 'normal', dilute solution showed only an enhancement of 2 under the same conditions.

Note that only one of the studies reported in Table 1 was done using a frozen solution. In all other cases, the sample was first precipitated, which is often relatively easy for molecular assemblies, due to their high molecular weight. This highlights the importance of obtaining the highest possible absolute sensitivity, even in DNP conditions.

Another approach, which is greatly facilitated by DNP, is the investigation of biomolecules in their native cellular environments. While this is an attractive approach, it is also associated with several experimental difficulties, which is the reason why only a few examples of such DNP-supported studies of cellular preparations have been reported. This includes a membrane protein (Renault et al., 2012), a membrane-embedded protein complex (Kaplan et al., 2015), and a yeast prion protein (Frederick et al., 2015), overproduced in cells. The main difficulty of this approach is the complexity of the experimental NMR data, arising from overlaps with "background" signals from other components of the cell. This usually requires that either a dedicated labelling scheme (Kaplan et al., 2015) or a targeted approach (Frederick et al., 2015; Viennet et al., 2016) is employed. The obtained DNP enhancements of such cellular preparations are generally inferior to those for conventionally prepared samples. For these reasons, this methodology is not yet widely used, but is well suited to answer specific questions in comparison to *in vitro* data, or to validate an *in vitro* model in a cellular setting.

The composition and particularly the deuteration level of the cryo-protectant matrix has a significant effect on spin diffusion and consequently on the DNP enhancement. The most commonly used solvent composition is 60% glycerol-d_8/30% D_2O/10% H_2O (v/v/v, a.k.a "DNP juice"). However, many precipitated samples are not compatible with a high glycerol content, which results in re-dissolution. In these cases, the lowest possible glycerol concentration needs to be determined, which still provides cryo-protection and does not result in sample re-dissolution. Alternatively, other glass-forming solvents (such as mixtures of water and DMSO-d_6) may be explored. The deuteration level of the cryo-protectant matrix is usually adjusted by adding an appropriate amount of H_2O in otherwise deuterated cryoprotectant/D_2O background to yield the highest enhancement. For the molecular assembly studies reviewed here, the highest enhancements were obtained by using a fully deuterated matrix: ε_H of 65 at 600 MHz and 21 at 800 MHz using 30/70 % glycerol-d_8/D_2O and 70/30 % glycerol-d_8/D_2O, respectively (Sergeyev et al., 2017; Fricke et al., 2016). These results indicate that the small number of protons introduced with the protein is sufficient for an effective spin diffusion in samples of molecular assemblies.

The level of protein deuteration is another factor that affects the DNP enhancement by extending the longitudinal relaxation times, and it has been shown that protein perdeuteration provides superior DNP enhancements as compared to the same type of experiments in fully protonated samples (Akbey et al., 2010). This method requires that the protein of interest is expressed in a fully deuterated culture medium and that protons, which would serve as a magnetization source for cross-polarization, are re-introduced at exchangeable sites during protein purification by refolding in a protonated buffer. However, this approach has not been explored for molecular assemblies so far, due to difficulties in preparing perdeuterated samples of protein assemblies.

Finally, the radical concentration affects longitudinal and transverse relaxation as well as the DNP enhancement, which together have a dramatic effect on the intensity of NMR signals. Although some guidelines exist, the optimal concentration of the radical is system dependent, and is usually adjusted to provide the maximum signal-to-noise observed per unit time without additional line broadening (Lange et al., 2012). It is worth mentioning that in some cases the radical may bind to the protein, requiring the use of very low radical concentrations (Nagaraj et al., 2016). For molecular assemblies, the employed radical concentrations are between 8 and 28 mM (Table 1), with the majority of studies done using around 8-10 mM AMUPol.

2.4. Spectral resolution

Impressive sensitivity enhancement factors (ε_H), as high as ~210 (at 400 MHz, 100 K and 8.8 kHz MAS), have been reported on microcrystalline protein samples (Jagtap et al., 2016). This signal enhancement comes, however, at the expense of a substantial signal broadening, which compromises spectral resolution. The observed linewidths under various DNP conditions are also summarized in Table 1. Several studies have shown that this broadening is primarily inhomogeneous and associated with the low temperature required for DNP experiments, which results in freezing-out of different side chain conformers (Linden et al., 2011a; Siemer et al., 2012). Additional factors that contribute to this are the presence of paramagnetic radicals and the typically low magnetic field strength (400 MHz) and MAS rate (below 20 kHz) at which the experiments are usually performed.

Several directions have been explored to alleviate the resolution problem in DNP spectra of proteins. Akbey et al. (2012) introduced high-temperature DNP, which aims at increasing spectral resolution by performing experiments at temperatures of around 180 K instead of 100 K. At this temperature only modest enhancements of 11-18 were obtained (at 400 MHz). However, the resolution was shown to be similar to room temperature spectra for some favorable sites in deuterated microcrystalline SH3. More recently, Barnes and coworkers developed an alternative approach, aimed at removing the deleterious effects on NMR signals produced by paramagnetic DNP polarizing agents. They notably demonstrated that electron decoupling produces a significant reduction in ^{13}C line widths of [^{13}C,^{15}N]urea mixed with Trityl experiments under magic angle spinning (Saliba et al, 2017; Sesti et al, 2018).

Another possibility to partly restore spectral resolution of biological solids is to perform the DNP experiments at high magnetic fields (600 and 800 MHz), where the homogeneous component of the line broadening is reduced (Lopez del Amo et al., 2013). Lange, Baldus and co-workers showed that a significant increase in resolution can be attained by doubling the magnetic field strength from 400 to 800 MHz, thereby allowing detailed structural investigation of the membrane protein KcsA in different functional states and of the type III secretion needles (T3SS) (Fricke et al., 2016; Koers et al., 2014). However, this approach is also accompanied by a reduction in DNP enhancements and a maximum enhancement of 21 at 800 MHz was obtained on the T3SS. A smaller reduction in the DNP enhancement paralleled with smaller gains in resolution has been obtained at 600 MHz magnetic field strength suggesting that this magnetic field might be a good compromise for DNP of biomolecular assemblies, yielding increased resolution with reasonably high enhancement (Fricke et al., 2014; Gupta et al., 2016; Sergeyev et al., 2017).

The benefits of faster sample spinning (up to 40 kHz) were recently investigated. Sergeyev et al. (2017) showed on the coat protein of Pf1 virus that DNP at 600 MHz and 25 kHz MAS results in peaks sharper than in the slow spinning regime and in improvements in signal-to-noise due to better microwave penetration, enabling novel experiments with multiple inter-nuclear transfers and long mixing times for efficient backbone and side chain assignment. More recently, Jaudzems and coworkers reported that high quality spectra of the *Acinetobacter phage* 205 (AP205) nucleocapsid could be obtained by combining 800 MHz magnetic field strength with 40 kHz MAS and high power proton decoupling (Jaudzems

et al. 2018). DNP enhanced carbon-13 NMR linewidths of less than 1 ppm were reported on AP205, and the authors additionally showed that a significant reduction of the homogeneous contribution to the line broadening was obtained by increasing the MAS rates (from 10 to 40 kHz) and the proton decoupling field strengths (from 100 to 150 kHz). This effect was explained as the result of an improved averaging of the anisotropic interactions and of the paramagnetic couplings with the radical. While this improvement is masked by inhomogeneous broadening in the observed linewidths, it does nonetheless guarantee long coherence lifetimes, allowing in turn the acquisition of scalar-based experiments.

In summary, DNP can enhance protein NMR signals by up to two orders of magnitude. However, a major bottleneck, which prevents its widespread application to protein structural studies is the deterioration of spectral resolution at the DNP experimental conditions. Although the resolution can be improved by performing experiments at higher temperatures and higher magnetic fields, these approaches yield today reduced enhancements. In this sense, increasing the MAS frequency seems to be appealing as it provides both improved resolution and high signal-to-noise ratios in the case of densely packed multi-component assemblies. High temperature DNP has not shown its potential so far for molecular assemblies.

3. Application to structure and dynamics characterization of molecular assemblies

The increased sensitivity provided by DNP has allowed one to perform structural investigations on molecular assemblies that would otherwise have been impossible due to prohibitively long experimental times, often yielding unprecedented structural information, missing in conventional room temperature MAS NMR measurements. In this section, we recapitulate these findings and highlight the additional benefits obtained by DNP in the structural studies of viral capsids, and of the type III and IV bacterial secretion systems.

3.1. Viral capsids

To date three different types of viral assemblies have been successfully characterized using DNP-enhanced solid-state NMR, suggesting that DNP is uniquely positioned for viral capsid structural studies. This concerns the tubular assemblies of the HIV-1 capsid protein (CA) and its maturation intermediate (CA-SP1) (Gupta et al., 2016), the filamentous bacteriophage Pf1 formed by helical assemblies of the coat protein wrapping up the viral DNA (Sergeyev et al., 2011; Sergeyev et al., 2017) and the icosahedral capsid assembly of the *Acinetobacter phage 205* (AP205) coat protein (Jaudzems et al., 2018).

The DNP experiments on HIV-1 CA and CA-SP1 assemblies allowed to directly observe functionally important residues that were invisible in room-temperature dipolar-based MAS NMR spectroscopy, cryo-EM and X-ray measurements because of dynamic disorder. This included the observation of most of the resonances of the SP1 peptide residues in the CA-SP1 maturation intermediate, multiple side-chain conformers for several residues and unique correlations arising from intermolecular interactions (**Figure 1**). The SP1 peptide resonances could be assigned based on a single DARR measurement and their chemical shifts indicated a helical conformation. While similar indications were obtained previously based on cryo-EM data of the in vitro assembled CA-SP1 capsids from Rous sarcoma virus, where electron density associated with SP1 could not be seen, the DNP NMR spectra provided a direct experimental evidence of the presence of the minor helical conformer. In addition, residues in the hinge region of CA, which play a critical role in capsid assembly and are difficult to detect at 253-277 K due to millisecond timescale dynamics, were readily observed and assigned in the DNP spectra. An intermolecular correlation between a key hinge residue, Y145 and R162, was also identified illustrating how DNP can provide critical restraints for structure determination of capsid assemblies.

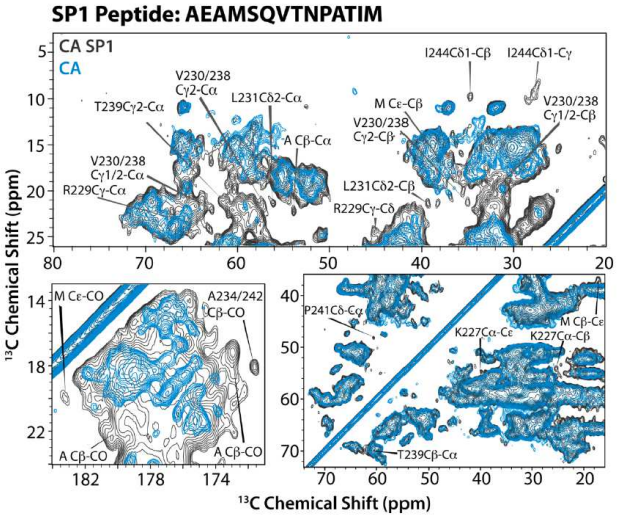

Figure 1. Amino acid sequence of the SP1 peptide and an overlay of DNP-enhanced ^{13}C–^{13}C DARR spectra at 109 K and 600 MHz of tubular assemblies of U-^{13}C,^{15}N CA (blue) and CA-SP1 (black). The MAS frequency was 12.5 kHz, and the mixing time was 40 ms. Assigned SP1 resonances are labeled by residue name and number. Adapted with permission from Gupta et al., 2016. Copyright 2016 American Chemical Society.

Two detailed DNP studies of the Pf1 bacteriophage have been reported in the literature. The first aimed at assigning the chemical shifts of the unusual DNA structure in the Pf1 virion (Sergeyev et al., 2011), while the second proposed a novel DNP-enabled backbone assignment strategy (Sergeyev et al., 2017). The DNA peaks were faintly observable in ssNMR spectra acquired at 213-243 K, and their assignment had been nearly impossible. With a 22-fold enhancement from DNP, these peaks could be clearly resolved and assigned for the first time. This assignment revealed extreme chemical shift values indicative of an unusual DNA structure (**Figure 2**), lacking hydrogen bonding but involving some type of aromatic ring interaction. The complete *de novo* assignment of the coat protein of Pf1 virus in the frozen state near 100 K has been achieved by combining the sensitivity benefits of DNP, fast MAS and non-uniform sampling, with the introduction of a new sequential side-chain-side-chain correlation method. Comparison of DNP and conventional NMR data collected near 100 and 273 K respectively showed ^{13}C and ^{15}N chemical shift perturbations into distinct regions of the protein, concomitant with a broadening of the lines. Correlations could be established between the temperature-induced perturbations and the hydration maps of the viral assembly, allowing rationalization in terms of solvation phenomena.

More recently, high quality DNP-enhanced NMR spectra of the *Acinetobacter phage* 205 (AP205) nucleocapsid could be obtained at high magnetic field (800 MHz) and fast MAS (40 kHz). These spectra enabled the assignment of aromatic resonances of the coat protein and its packaged RNA, which are not observed at room temperature. In particular, several new aromatic-to-aliphatic and aromatic-to-aromatic contacts were detected, which could be used to refine the 3D structure of the protein (Jaudzems et al., 2018). Although site-specific internuclear proximities had been already measured under DNP conditions in assemblies reconstituted from differently labelled components, (Bayro et al., 2011; Maciejko et al., 2015) this study represents the first example where data extracted from DNP-enhanced spectra were constructively used in a structure determination on a uniformly labelled system.

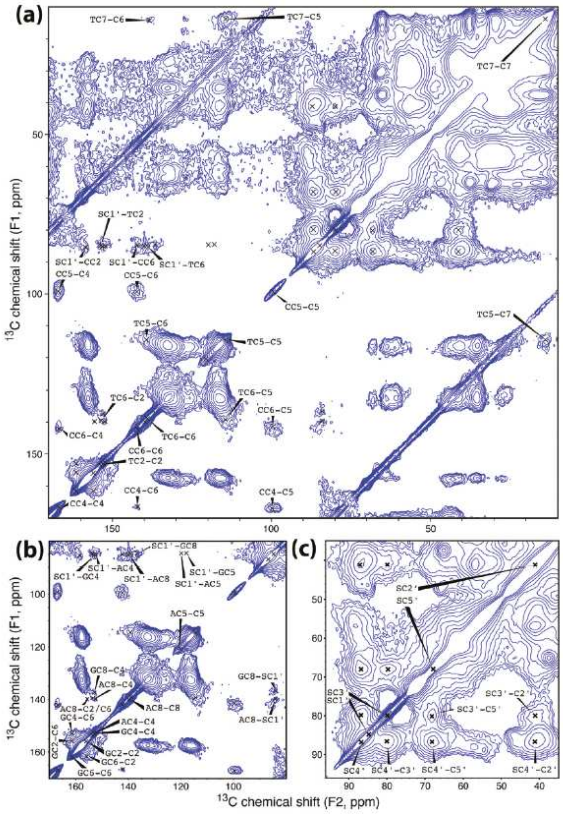

Figure 2. DNP-enhanced SSNMR spectra of Pf1 showing (a) the assignments of the dC/dT base resonances, (b) the dA/dG base resonances, and (c) the sugar spin systems. Data were collected using a 400 MHz wide-bore AVANCE III spectrometer at cryogenic temperatures (100 K), with a mixing time of 22 ms. Adapted with permission from Sergeyev 2011. Copyright 2011 American Chemical Society.

3.2. Other large protein complexes

In recent years, exciting applications of DNP-enhanced solid-state NMR to large molecular assemblies other than viruses appeared. DNP has thus been applied to bacterial secretion systems (T3SS or T4SS) by the groups of Lange (Fricke et al., 2014; Fricke et al., 2016) and Baldus (Kaplan et al., 2015). As previously mentioned, the seminal work by Fricke and co-workers was very instructive concerning factors that determine line width in DNP NMR spectra (Fricke et al., 2014). Here, the T3SS needles investigated are formed by rings of the protein MxiH whose structure shows two helices, helix one being located at the outer surface of the filamentous needle, and helix two at the inside of the ring. It turns out that under DNP conditions at 14.1 T and 104 K, using TOTAPOL (ε = 23), a sub-spectrum of sharper lines is observed that stems from the inner ring. The favorable line width observed for signals of residues in the inner ring is influenced by a locking of their side chains due to space restrictions, avoiding the formation of conformers and thus the appearance of heterogeneous broadening at the measurement temperatures used, and presumably also a larger distance to radicals. Later, the same system was investigated at a field strength of 18 T at 95 K and using AMUPol as radical, yielding an enhancement of ε = 21 (Fricke et al., 2016). On the whole, a very similar spectrum was observed, however the resolved signals showed improved resolution (the line width was reduced by 22%), demonstrating thus a contribution of homogeneous broadening due to the presence of the radicals. The application of DNP enabled an investigation of a T4 secretion system core complex *in vivo* (Kaplan et al., 2015), where it was found that it acquires a more compact structure than *in vitro*.

As an example of a large molecular machine that would defy NMR investigations under non-DNP conditions, aspects of ribosome structure were investigated. A first seminal investigation (Gelis et al., 2013) demonstrated the feasibility of DNP applications to the ribosome (ε = 25), and showed suitable line width by means of selectively labelled samples. A second investigation was focused on the structure of the nascent chain inside the exit tunnel (Lange et al., 2016). Here, the DsbA signal peptide was fused to the SecM stalling signal to generate ribosomes with the same nascent chain, and the expression protocol ensured its exclusive labelling with ^{13}C and ^{15}N. ^{13}C-double-quantum versus single-quantum spectra were recorded and the observed chemical shifts for isoleucine, valine, proline and serine residues interpreted with respect to the indicated secondary structure. It was shown that the DsbA signal peptide as nascent chain does not form a helix inside the ribosome tunnel and in consequence very unlikely to be influencing the surface of the ribosome with regards to promoting binding of factors co-translationally binding to the nascent chain.

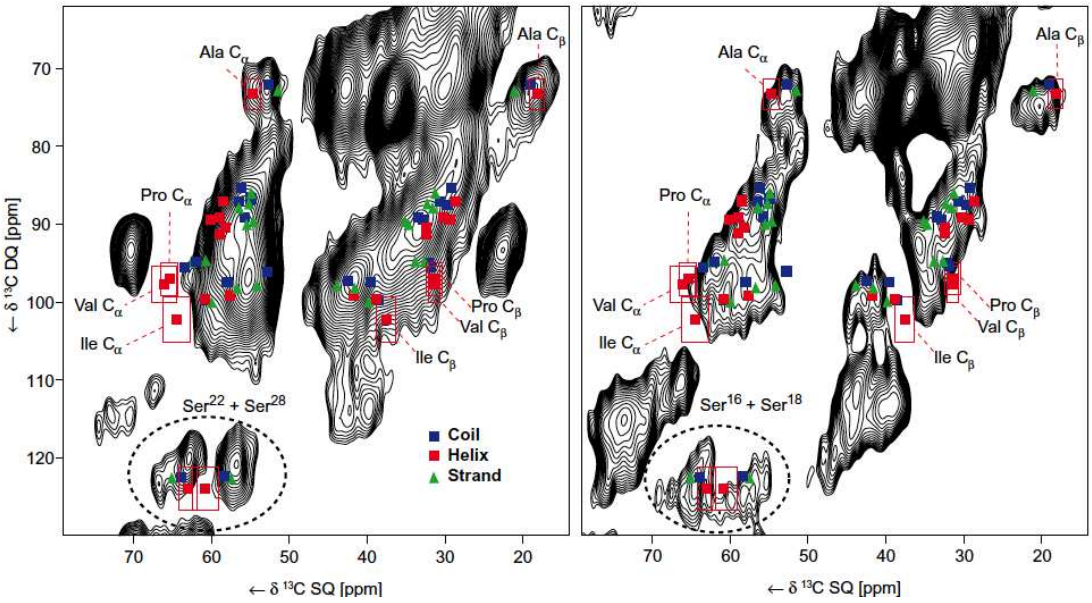

Figure 3. POST-C7 DQ-SQ spectra of the ribosome embedded nascent chain S16A/S18A-DsbA-SecM (left panel) and S22A/S28A-DsbA-SecM (right panel). Averaged chemical shifts for helical (red squares), strand-like (blue squares), or coil-like (green triangles) geometries are shown (35). Well-separated cross peak patterns of amino acids that do not strongly overlap with other residue types are labeled accordingly. Acquisition in the direct and indirect dimension was 20 ms (1582 points) and 2 ms (128 points), respectively. Adapted with permission from Lange 2016.

3.3. Membrane proteins

A surprisingly large number of fruitful DNP MAS NMR investigations of membrane proteins appeared in the last few years, covering retinal-containing photoreceptors (Bajaj et al., 2009; Becker-Baldus et al., 2015; Maciejko et al., 2015; Mehler et al., 2017; Stöppler et al., 2016) a G-protein-coupled receptor (Joedicke et al., 2018), neurotoxin II bound to a ligand-gated ion channel (Linden et al., 2011b), and transporters (Lehnert et al., 2016; Ong et al., 2013; Spadaccini et al., 2018), illustrating the potential of DNP MAS NMR to the wide field of membrane proteins. Since such proteins may be investigated in frozen detergent solutions, after incorporation into liposomes, or when still embedded in native membranes, a variety of approaches were tested. In some cases, the application of DNP appeared natural and did not bring about additional complications, because the respective preparations needed to be investigated in the frozen state anyways for reasons of unfavourable protein

dynamics interfering with MAS NMR requirements (especially those dissolved in detergent solutions and some samples involving proteoliposomes). With regards to the DNP-specific measurement conditions, the glycerol content was often optimized to an appropriately low amount, choosing mostly 30%, or sometimes even less. In individual cases, radicals were added without glycerol to the membrane protein samples that were equilibrated in an appropriate H_2O/D_2O mixture after preparation. In investigations of the photoactive proteins, signal enhancements in the range of 30-60 are reported at 9.4 T when using AMUPol together with a reduced amount of glycerol. The highest enhancement was reported in an investigation of the bradykinin receptor in frozen detergent solutions (ε = 169, AMUPol).

In a seminal paper on bacteriorhodopsin within intact purple membranes, the group of Griffin reported additional sets of signals occurring upon trapping photointermediates at low temperatures (Bajaj et al., 2009), in particular four sets for the L state. In this case, a field strength less than 9 T and TOTAPOL were employed, yielding enhancements in the range of 90 at 90 K. The very stable purple membranes were kept in 60% d_8-glycerol for the measurements. Investigations on channelrhodopsins (Becker-Baldus et al., 2015; Stöppler et al., 2016) in proteoliposomes of phosphatidylcholine or POPC/POPG/Cholesterol aimed at determining the isomer composition in the long-term dark state, finding more than 95% *all-trans* retinal in contrast to earlier biochemical investigations, and to detect intermediates of the photocycle. The group of Glaubitz was successful in determining intermolecular contacts within proteorhodopsin pentamers (Maciejko et al., 2015), using mixed samples of ^{15}N and ^{13}C labelled protein in DMPC/DMPA proteoliposomes, and applying 30% v/v glycerol as cryoprotectant. Measurements of such heteronuclear interactions in mixed or diluted samples require sufficient signal-to-noise, and DNP was critical to this end. In a second investigation on proteorhodopsin, deviations of retinal structure from an ideal planar arrangement were detected with the help of DNP (Mehler et al., 2017).

Several transporters were studied by DNP NMR with a focus on mechanism. An investigation on the secondary transporter EmrE was set out to test the effects of substrate binding under DNP conditions (Ong et al., 2013), using DMPC proteoliposomes, reporting an enhancement of 19 at 9 T. Conformational changes in the ABC transporter MsbA embedded in DMPC/DMPA liposomes, in particular a movement of helices 4 and 6, were reported in connection with ligand binding and ATP hydrolysis (Spadaccini et al., 2018). A landmark investigation concerned peptide binding to the detergent-solubilized transporter associated with antigen processing (TAP) (Lehnert et al., 2016), and included the derivation of an atomic-resolution structural model of a bound peptide, revealing interactions critical for TAP binding and allowing to explain substrate selection rules.

An example for the investigation of a membrane protein embedded in whole membrane patches is given by the Reif laboratory (Jacso et al., 2012). There, the protein *mistic* contained ^{13}C-labelled glycine, serine, threonine, and valine, and was expressed into *E. coli* membranes to demonstrate that it adopts α-helical structure in this environment. Membrane patches were purified and directly subjected to DNP MAS NMR measurements with no glycerol added, yielding spectra that enabled an analysis of the backbone and Cβ chemical shifts with regards to the adopted secondary structure. The application of 20-40 mM TOTAPol as radical yielded enhancements in the range of 15-30.

Recently, the conformations of ligands bound to certain subtypes of the bradykinin receptor were determined by solid-state NMR under DNP conditions (Joedicke et al., 2018). Dilute but frozen detergent solutions of the receptor were employed, containing 50% v/v d_8-glycerol, hence the application of DNP was critical and the large enhancement of ε = 169 was absolutely welcome. To obtain resonance assignments, peptides were labelled at individual sites, employing labelling of one or two amino acids, and structures calculated on the basis of dihedral angles derived from the chemical shifts of backbone atoms and Cβ.

Conclusion: With the introduction of highly efficient polarization sources and fast MAS cryogenic probes, MAS DNP enhanced biomolecular NMR spectroscopy has recently greatly matured. As exemplified by the applications described above, it has become an effective and relevant technique for the structural investigation of biological assemblies, in the (several) cases where conventional room temperature NMR lacks sensitivity. The broadening of the NMR lines observed systematically at cryogenic temperatures (together with the today's scarcity of very high-field DNP NMR spectrometers) so far hamper, however, an optimal and therefore broader use of this technique. In this context, the future development of new formulations or experimental approaches that will allow one to maintain a high signal enhancement factor with no penalty in spectral resolution appear highly strategic.

Acknowledgements: KJ is supported by a MC incoming fellowship (REA grant agreement n°661175 "virus-DNP-NMR").

Table 1. Experimental conditions used for DNP-enhanced NMR studies of various molecular assemblies

Sample	Preparation	Matrix/cryo-protectant composition	Radical	Labeling	B_0 (MHz)	MAS (kHz)	T (K)	ε (^{1}H-^{13}C CP)	^{13}C linewidths (ppm)	Source
Pf1	PEG-8000 precipitate	40/50/10 % (v/v/v) DMSO-d6/D2O/H2O, and 20% w/v PEG-8000.	20 μM TOTAPOL	uniform 13C- and 15N	400		100	17/22	1.8, average 2.4	(Sergeyev et al., 2011)
Pf1	PEG-8000 precipitate	30/70 % glycerol-d8/D2O	10 mM AMUPol	uniform 13C- and 15N	600	11	98-106	35	1.3	(Sergeyev et al., 2017)
Pf1	PEG-8000 precipitate	30/70 % glycerol-d8/D2O	10 mM AMUPol	uniform 13C- and 15N	600	25	98-108	65		(Sergeyev et al., 2017)
HIV-1 CA-SP1-NC protein	Frozen protein solution	50/37.5/12.5 % (v/v/v) glycerol-d8/D2O/H2O	10 mM TOTAPOL	uniform 13C- and 15N	400	8.9	110/182	20/2		(Gupta et al., 2016)
HIV-1 CA protein	Sedimented tubular assemblies	20/80 % (v/v) glycerol-d8/H2O	8 mM AMUPol	uniform 13C- and 15N	600	12.5	109/180	64/20		(Gupta et al., 2016)
HIV-1 CA-SP1 protein	Sedimented tubular assemblies	20/80 % (v/v) glycerol-d8/H2O	8 mM AMUPol	uniform 13C- and 15N	600	12.5	109	20	(0.5) 1.5-2.0	(Gupta et al., 2016)
HIV-1 CA protein	Sedimented tubular assemblies	20/80 % (v/v) glycerol-d8/H2O	8 mM TOTAPOL	uniform 13C- and 15N	800	10	110	4		(Gupta et al., 2016)
HIV-1 CA protein	Sedimented tubular assemblies	20/80 % (v/v) glycerol-d8/H2O	8 mM AMUPol	uniform 13C- and 15N	800	10	110	4		(Gupta et al., 2016)
HIV-1 CA-SP1-NC protein	Sedimented tubes and cones	20/72/8 % (v/v) glycerol-d8/D2O/H2O	8 mM AMUPol	uniform 13C- and 15N	800	10	110	7-11		(Gupta et al., 2016)
AP205	Microcrystalline	16% (w/v) deuterated PEG-4600	10 mM AMUPol	uniform 13C- and 15N	400	12.5	107	82	1.9-2.8	(Jaudzems et al., 2018)
AP205	Microcrystalline	16% (w/v) deuterated PEG-4600	10 mM AMUPol	uniform 13C- and 15N	800	12	103	16	1.1-1.8	(Jaudzems et al., 2018)
AP205	Microcrystalline	16% (w/v) deuterated PEG-4600	10 mM AMUPol	uniform 13C- and 15N	800	40	115	17	1.0-1.7	(Jaudzems et al., 2018)
MxiH needles	In vitro polymerized needles	72/25/3 % (v/v/v) glycerol-d8/D2O/H2O	28 mM TOTAPOL	uniform 13C- and 15N	600	11	104	23	1.1–2.2	(Fricke et al., 2014)
MxiH needles	In vitro polymerized needles	70/30 % (v/v) glycerol-d8/D2O	14 mM AMUPol	uniform 13C- and 15N	800	8	95	21	0.9–1.8	(Fricke et al., 2016)
T4SScc	Cell-embedded protein complex	1) 45/32.5/22.5 % (v/v/v) glycerol-d8/D2O/H2O 2) 22.5/32.5/42.5 % (v/v/v) glycerol-d8/D2O/H2O	20 mM AMUPol	selective 13C,15N-Gly, Ser, Leu, Val or selective 13C,15N-Thr, Val	400	8	100	60		(Kaplan et al., 2015)
T4SScc	Cell-embedded protein complex				800	8	100	15	1.5	(Kaplan et al., 2015)

E.coli 70S ribosome	Sedimented particles	60/30/10 % (v/v/v) glycerol-d8/D2O/H2O	20 mM TOTAPOL	unlabeled	400	8	100	25		(Gelis et al., 2013)
E.coli 70S ribosome	Sedimented particles	30% (w/v) sucrose in 90/10% (v/v) D2O/H2O	20 mM TOTAPOL	unlabeled	400	8	100	13		(Gelis et al., 2013)
E.coli 30S-IF1 complex	Sedimented particles	60/30/10 % (v/v/v) glycerol-d8/D2O/H2O	20 mM TOTAPOL	uniform 13C- and 15N or selective 13C,15N-Tyr, His	400	8	100	25	1.0-1.2	(Gelis et al., 2013)
Ribosome-nascent chain complex	Sedimented particles	60/30/10 % (v/v/v) glycerol-d8/D2O/H2O	30 mM TOTAPOL	unlabeled ribosome carrying uniformly 13C,15N–labeled DsbA-SecM peptide	400	8.9	105	15-20		(Lange et al., 2016)

References

Albert, B. J., Gao, C., Sesti, E. L., Saliba, E. P., Alaniva, N., Scott, F. J., Sigurdsson, S. T., Barnes, A. B. Dynamic Nuclear Polarization Nuclear Magnetic Resonance in Human Cells Using Fluorescent Polarizing Agents. Biochemistry 2018, 57 (31), 4741–4746.

Akbey, U., Oschkinat, H., 2016. Structural biology applications of solid state MAS DNP NMR. J. Magn. Reson. 269, 213-224.

Akbey, U., Linden, A.H., Oschkinat, H., 2012. High-Temperature Dynamic Nuclear Polarization Enhanced Magic-Angle-Spinning NMR. Appl. Magn. Reson. 43, 81-90.

Akbey, U., Franks, W.T., Linden, A., Lange, S., Griffin, R.G., van Rossum, B.J., Oschkinat, H., 2010. Dynamic nuclear polarization of deuterated proteins. Angew. Chem. Int. Ed. Engl. 49, 7803-7806.

Bajaj, V.S., Mak-Jurkauskas, M.L., Belenky, M., Herzfeld, J., Griffin, R.G., 2009. Functional and shunt states of bacteriorhodopsin resolved by 250 GHz dynamic nuclear polarization-enhanced solid-state NMR. Proc. Natl. Acad. Sci. U.S.A. 106, 9244-9249.

Bajaj, V.S., Farrar, C.T., Hornstein, M.K., Mastovsky, I., Vieregg, J., Bryant, J., Elena, B., Kreischer, K.E., Temkin, R.J., Griffin, R.G., 2003. Dynamic nuclear polarization at 9T using a novel 250GHz gyrotron microwave source. J. Magn. Reson. 160, 85-90.

Barnes, A.B., Markhasin, E., Daviso, E., Michaelis, V.K., Nanni, E.A., Jawla, S.K., Mena, E.L., DeRocher, R., Thakkar, A., Woskov, P.P., Herzfeld, J., Temkin, R.J., Griffin, R.G., 2012. Dynamic nuclear polarization at 700 MHz/460 GHz. J. Magn. Reson. 224, 1-7.

Bayro, M.J., Debelouchina, G.T., Eddy, M.T., Birkett, N.R., MacPhee, C.E., Rosay, M., Maas, W.E., Dobson, C.M., Griffin, R.G., 2011. Intermolecular Structure Determination of Amyloid Fibrils with Magic-Angle Spinning and Dynamic Nuclear Polarization NMR. J. Am. Chem. Soc. 133, 13967-13974.

Becker-Baldus, J., Bamann, C., Saxena, K., Gustmann, H., Brown, L.J., Brown, R.C.D., Reiter, C., Bamberg, E., Wachtveitl, J., Schwalbe, H., Glaubitz, C., 2015. Enlightening the photoactive site of channelrhodopsin-2 by DNP-enhanced solid-state NMR spectroscopy. Proc. Natl. Acad. Sci. U.S.A. 112, 9896-9901.

Can, T.V., Ni, Q.Z., Griffin, R.G., 2015. Mechanisms of dynamic nuclear polarization in insulating solids. J. Magn. Reson. 253, 23-35.

Can, T.V., Caporini, M.A., Mentink-Vigier, F., Corzilius, B., Walish, J.J., Rosay, M., Maas, W.E., Baldus, M., Vega, S., Swager, T.M., Griffin, R.G., 2014. Overhauser effects in insulating solids. J. Chem. Phys. 141, 064202.

Debelouchina, G.T., Bayro, M.J., van der Wel, P.C.A., Caporini, M.A., Barnes, A.B., Rosay, M., Maas, W.E., Griffin, R.G., 2010. Dynamic nuclear polarization-enhanced solid-state NMR spectroscopy of GNNQQNY nanocrystals and amyloid fibrils. Phys. Chem. Chem. Phys. 12, 5911-5919.

Fernandez-de-Alba, C., Takahashi, H., Richard, A., Chenavier, Y., Dubois, L., Maurel, V., Lee, D., Hediger, S., De Paepe, G., 2015. Matrix-free DNP-enhanced NMR spectroscopy of liposomes using a lipid-anchored biradical. Chem. Eur. J. 21, 4512-4517.

Frederick, K.K., Michaelis, V.K., Corzilius, B., Ong, T.C., Jacavone, A.C., Griffin, R.G., Lindquist, S., 2015. Sensitivity-enhanced NMR reveals alterations in protein structure by cellular milieus. Cell 163, 620-628.

Frederick, K.K., Michaelis, V.K., Caporini, M.A., Andreas, L.B., Debelouchina, G.T., Griffin, R.G., Lindquist, S., 2017. Combining DNP NMR with segmental and specific labeling to study a yeast prion protein strain that is not parallel in-register. Proc. Natl. Acad. Sci. U.S.A. 114, 3642-3647.

Fricke, P., Demers, J.P., Becker, S., Lange, A., 2014. Studies on the MxiH Protein in T3SS Needles Using DNP-Enhanced ssNMR Spectroscopy. Chemphyschem 15, 57-60.

Fricke, P., Mance, D., Chevelkov, V., Giller, K., Becker, S., Baldus, M., Lange, A., 2016. High resolution observed in 800 MHz DNP spectra of extremely rigid type III secretion needles. J. Biomol. NMR 65, 121-126.

Geiger, M.A., Orwick-Rydmark, M., Marker, K., Franks, W.T., Akhmetzyanov, D., Stoppler, D., Zinke, M., Specker, E., Nazare, M., Diehl, A., van Rossum, B.J., Aussenac, F., Prisner, T., Akbey, U., Oschkinat, H., 2016a. Temperature dependence of cross-effect dynamic nuclear polarization in rotating solids: advantages of elevated temperatures. Phys. Chem. Chem. Phys. 18, 30696-30704.

Geiger, Y., Gottlieb, H.E., Akbey, U., Oschkinat, H., Goobes, G., 2016b. Studying the Conformation of a Silaffin-Derived Pentalysine Peptide Embedded in Bioinspired Silica using Solution and Dynamic Nuclear Polarization Magic-Angle Spinning NMR. J. Am. Chem. Soc. 138, 5561-5567.

Gelis, I., Vitzthum, V., Dhimole, N., Caporini, M.A., Schedlbauer, A., Carnevale, D., Connell, S.R., Fucini, P., Bodenhausen, G., 2013. Solid-state NMR enhanced by dynamic nuclear polarization as a novel tool for ribosome structural biology. J. Biomol. NMR 56, 85-93.

Gupta, R., Lu, M.M., Hou, G.J., Caporini, M.A., Rosay, M., Maas, W., Struppe, J., Suiter, C., Ahn, J., Byeon, I.J.L., Franks, W.T., Orwick-Rydmark, M., Bertarello, A., Oschkinat, H., Lesage, A., Pintacuda, G., Gronenborn, A.M., Polenova, T., 2016. Dynamic Nuclear Polarization Enhanced MAS NMR Spectroscopy for Structural Analysis of HIV-1 Protein Assemblies. J. Phys. Chem. B 120, 329-339.

Jacso, T., Franks, W.T., Rose, H., Fink, U., Broecker, J., Keller, S., Oschkinat, H., Reif, B., 2012. Characterization of Membrane Proteins in Isolated Native Cellular Membranes by Dynamic Nuclear Polarization Solid-State NMR Spectroscopy without Purification and Reconstitution. Angew. Chem. Int. Ed. 51, 432-435.

Jagtap, A.P., Geiger, M.A., Stoppler, D., Orwick-Rydmark, M., Oschkinat, H., Sigurdsson, S.T., 2016. bcTol : a highly water-soluble biradical for efficient dynamic nuclear polarization of biomolecules. Chem. Commun. 52, 7020-7023.

Jantschke, A., Koers, E., Mance, D., Weingarth, M., Brunner, E., Baldus, M., 2015. Insight into the Supramolecular Architecture of Intact Diatom Biosilica from DNP-Supported Solid-State NMR Spectroscopy. Angew. Chem. Int. Ed. Engl. 54, 15069-15073.

Jaudzems, K., Bertarello, A., Chaudhari, S.R., Pica, A., Cala-De Paepe, D., Barbet-Massin, E., Pell, A.J., Akopjana, I., Kotelovica, S., Gajan, D., Ouari, O., Tars, K., Pintacuda, G., Lesage, A., 2018. Dynamic nuclear polarization enhanced biomolecular NMR spectroscopy at high magnetic field with fast magic-angle spinning. Angew. Chem. Int. Ed. Engl., accepted.

Joedicke, L., Mao, J., Kuenze, G., Reinhart, C., Kalavacherla, T., Jonker, H.R.A., Richter, C., Schwalbe, H., Meiler, J., Preu, J., Michel, H., Glaubitz, C., 2018. The molecular basis of subtype selectivity of human kinin G-protein-coupled receptors. Nat. Chem. Biol. 14, 284-290.

Kaplan, M., Cukkemane, A., van Zundert, G.C.P., Narasimhan, S., Daniels, M., Mance, D., Waksman, G., Bonvin, A.M.J.J., Fronzes, R., Folkers, G.E., Baldus, M., 2015. Probing a cell-embedded megadalton protein complex by DNP-supported solid-state NMR. Nat. Methods 12, 649-652.

Kaushik, M., Bahrenberg, T., Can, T. V.; Caporini, M. A., Silvers, R., Heiliger, J. X. R., Smith, A. A., Schwalbe, H., Griffin, R. G., Corzilius, B., 2016. Gd(III) and Mn(II) complexes for dynamic nuclear polarization: small molecular chelate polarizing agents and applications with site-directed spin labeling of proteins. Phys. Chem. Chem. Phys. 18, 27205–27218.

Koers, E.J., van der Cruijsen, E.A.W., Rosay, M., Weingarth, M., Prokofyev, A., Sauvee, C., Ouari, O., van der Zwan, J., Pongs, O., Tordo, P., Maas, W.E., Baldus, M., 2014. NMR-based structural biology enhanced by dynamic nuclear polarization at high magnetic field. J. Biomol. NMR 60, 157-168.

Lange, S., Linden, A.H., Akbey, U., Franks, W.T., Loening, N.M., van Rossum, B.J., Oschkinat, H., 2012. The effect of biradical concentration on the performance of DNP-MAS-NMR. J. Magn. Reson. 216, 209-212.

Lange, S., Franks, W.T., Rajagopalan, N., Doring, K., Geiger, M.A., Linden, A., van Rossum, B.J., Kramer, G., Bukau, B., Oschkinat, H., 2016. Structural analysis of a signal peptide inside the ribosome tunnel by DNP MAS NMR. Sci. Adv. 2, e1600379.

Lehnert, E., Mao, J., Mehdipour, A.R., Hummer, G., Abele, R., Glaubitz, C., Tampe, R., 2016. Antigenic Peptide Recognition on the Human ABC Transporter TAP Resolved by DNP-Enhanced Solid-State NMR Spectroscopy. J. Am. Chem. Soc. 138, 13967-13974.

Linden, A.H., Franks, W.T., Akbey, U., Lange, S., van Rossum, B.J., Oschkinat, H., 2011a. Cryogenic temperature effects and resolution upon slow cooling of protein preparations in solid state NMR. J. Biomol. NMR 51, 283-292.

Linden, A.H., Lange, S., Franks, W.T., Akbey, U., Specker, E., van Rossum, B.J., Oschkinat, H., 2011b. Neurotoxin II Bound to Acetylcholine Receptors in Native Membranes Studied by Dynamic Nuclear Polarization NMR. J. Am. Chem. Soc. 133, 19266-19269.

Lopez del Amo, J.M., Schneider, D., Loquet, A., Lange, A., Reif, B., 2013. Cryogenic solid state NMR studies of fibrils of the Alzheimer's disease amyloid-beta peptide: perspectives for DNP. J. Biomol. NMR 56, 359-363.

Maciejko, J., Mehler, M., Kaur, J., Lieblein, T., Morgner, N., Ouari, O., Tordo, P., Becker-Baldus, J., Glaubitz, C., 2015. Visualizing Specific Cross-Protomer Interactions in the Homo-Oligomeric Membrane Protein Proteorhodopsin by Dynamic-Nuclear-Polarization-Enhanced Solid-State NMR. J. Am. Chem. Soc. 137, 9032-9043.

Maly, T., Debelouchina, G. T., Bajaj, V. S., Hu, K. N., Joo, C. G., Mak-Jurkauskas, M. L., Sirigiri, J. R., van der Wel, P. C., Herzfeld, J., Temkin, R. J., Griffin, R. G., J. Chem. Phys. 2008, 128 (5), 052211.

Mathies, G., Caporini, M.A., Michaelis, V.K., Liu, Y., Hu, K.N., Mance, D., Zweier, J.L., Rosay, M., Baldus, M., Griffin, R.G., 2015. Efficient Dynamic Nuclear Polarization at 800 MHz/527 GHz with Trityl-Nitroxide Biradicals. Angew. Chem. Int. Ed. Engl. 54, 11770-11774.

Mehler, M., Eckert, C.E., Leeder, A.J., Kaur, J., Fischer, T., Kubatova, N., Brown, L.J., Brown, R.C.D., Becker-Baldus, J., Wachtveitl, J., Glaubitz, C., 2017. Chromophore Distortions in Photointermediates of Proteorhodopsin Visualized by Dynamic Nuclear Polarization-Enhanced Solid-State NMR. J. Am. Chem. Soc. 139, 16143-16153.

Mentink-Vigier, F., Paul, S., Lee, D., Feintuch, A., Hediger, S., Vega, S., De Paepe, G., 2015. Nuclear depolarization and absolute sensitivity in magic-angle spinning cross effect dynamic nuclear polarization. Phys. Chem. Chem. Phys. 17, 21824-21836.

Nagaraj, M., Franks, T.W., Saeidpour, S., Schubeis, T., Oschkinat, H., Ritter, C., van Rossum, B.J., 2016. Surface Binding of TOTAPOL Assists Structural Investigations of Amyloid

Fibrils by Dynamic Nuclear Polarization NMR Spectroscopy. Chembiochem 17, 1308-1311.
Ni, Q.Z., Daviso, E., Can, T.V., Markhasin, E., Jawla, S.K., Swager, T.M., Temkin, R.J., Herzfeld, J., Griffin, R.G., 2013. High frequency dynamic nuclear polarization. Acc. Chem. Res. 46, 1933-1941.
Ong, Y.S., Lakatos, A., Becker-Baldus, J., Pos, K.M., Glaubitz, C., 2013. Detecting substrates bound to the secondary multidrug efflux pump EmrE by DNP-enhanced solid-state NMR. J. Am. Chem. Soc. 135, 15754-15762.
Potapov, A., Yau, W.M., Ghirlando, R., Thurber, K.R., Tycko, R., 2015. Successive Stages of Amyloid-beta Self-Assembly Characterized by Solid-State Nuclear Magnetic Resonance with Dynamic Nuclear Polarization. J. Am. Chem. Soc. 137, 8294-8307.
Ravera, E., Corzilius, B., Michaelis, V.K., Luchinat, C., Griffin, R.G., Bertini, I., 2014. DNP-Enhanced MAS NMR of Bovine Serum Albumin Sediments and Solutions. J. Phys. Chem. B 118, 2957-2965.
Ravera, E., Corzilius, B., Michaelis, V.K., Rosa, C., Griffin, R.G., Luchinat, C., Bertini, I., 2013. Dynamic Nuclear Polarization of Sedimented Solutes. J. Am. Chem. Soc. 135, 1641-1644.
Ravera, E., Michaelis, V.K., Ong, T.C., Keeler, E.G., Martelli, T., Fragai, M., Griffin, R.G., Luchinat, C., 2015. Biosilica-Entrapped Enzymes Studied by Using Dynamic Nuclear-Polarization-Enhanced High-Field NMR Spectroscopy. Chemphyschem.
Renault, M., Pawsey, S., Bos, M.P., Koers, E.J., Nand, D., Tommassen-van Boxtel, R., Rosay, M., Tommassen, J., Maas, W.E., Baldus, M., 2012. Solid-State NMR Spectroscopy on Cellular Preparations Enhanced by Dynamic Nuclear Polarization. Angew. Chem. Int. Ed. Engl. 51, 2998-3001.
Rogawski, R., Sergeyev, I.V., Li, Y., Ottaviani, M.F., Cornish, V., McDermott, A.E., 2017. Dynamic Nuclear Polarization Signal Enhancement with High-Affinity Biradical Tags. J. Phys. Chem. B 121, 1169-1175.
Rosay, M., Zeri, A.C., Astrof, N.S., Opella, S.J., Herzfeld, J., Griffin, R.G., 2001. Sensitivity-enhanced NMR of biological solids: dynamic nuclear polarization of Y21M fd bacteriophage and purple membrane. J. Am. Chem. Soc. 123, 1010-1011.
Rosay, M., Lansing, J.C., Haddad, K.C., Bachovchin, W.W., Herzfeld, J., Temkin, R.J., Griffin, R.G., 2003. High-frequency dynamic nuclear polarization in MAS spectra of membrane and soluble proteins. J. Am. Chem. Soc. 125, 13626-13627.
Saliba, E. P., Sesti, E. L., Scott, F. J., Albert, B. J., Choi, E. J., Alaniva, N., Gao, C., Barnes, A. B. Electron Decoupling with Dynamic Nuclear Polarization in Rotating Solids. J. Am. Chem. Soc. 2017, 139 (18), 6310–6313.
Sauvee, C., Rosay, M., Casano, G., Aussenac, F., Weber, R.T., Ouari, O., Tordo, P., 2013. Highly efficient, water-soluble polarizing agents for dynamic nuclear polarization at high frequency. Angew. Chem. Int. Ed. Engl. 52, 10858-10861.
Sauvee, C., Casano, G., Abel, S., Rockenbauer, A., Akhmetzyanov, D., Karoui, H., Siri, D., Aussenac, F., Maas, W., Weber, R.T., Prisner, T., Rosay, M., Tordo, P., Ouari, O., 2016. Tailoring of Polarizing Agents in the bTurea Series for Cross-Effect Dynamic Nuclear Polarization in Aqueous Media. Chemistry 22, 5598-5606.
Sergeyev, I.V., Day, L.A., Goldbourt, A., McDermott, A.E., 2011. Chemical Shifts for the Unusual DNA Structure in Pf1 Bacteriophage from Dynamic-Nuclear-Polarization-Enhanced Solid-State NMR Spectroscopy. J. Am. Chem. Soc. 133, 20208-20217.

Sergeyev, I.V., Itin, B., Rogawski, R., Day, L.A., McDermott, A.E., 2017. Efficient assignment and NMR analysis of an intact virus using sequential side-chain correlations and DNP sensitization. Proc. Natl. Acad. Sci. U.S.A. 114, 5171-5176.

Sesti, E. L., Saliba, E. P., Alaniva, N., Barnes, A. B. 2018. Electron decoupling with cross polarization and dynamic nuclear polarization below 6 K. J. Magn. Res., *295*, 1–5.

Siemer, A.B., Huang, K.Y., McDermott, A.E., 2012. Protein Linewidth and Solvent Dynamics in Frozen Solution NMR. Plos One 7.

Smith, A.N., Caporini, M.A., Fanucci, G.E., Long, J.R., 2015. A method for dynamic nuclear polarization enhancement of membrane proteins. Angew. Chem. Int. Ed. Engl. 54, 1542-1546.

Song, C., Hu, K.N., Joo, C.G., Swager, T.M., Griffin, R.G., 2006. TOTAPOL: a biradical polarizing agent for dynamic nuclear polarization experiments in aqueous media. J. Am. Chem. Soc. 128, 11385-11390.

Spadaccini, R., Kaur, H., Becker-Baldus, J., Glaubitz, C., 2018. The effect of drug binding on specific sites in transmembrane helices 4 and 6 of the ABC exporter MsbA studied by DNP-enhanced solid-state NMR. Biochim. Biophys. Acta 1860, 833-840.

Stöppler, D., Song, C., van Rossum, B.J., Geiger, M.A., Lang, C., Mroginski, M.A., Jagtap, A.P., Sigurdsson, S.T., Matysik, J., Hughes, J., Oschkinat, H., 2016. Dynamic Nuclear Polarization Provides New Insights into Chromophore Structure in Phytochrome Photoreceptors. Angew. Chem. Int. Ed. Engl. 55, 16017-16020.

Su, Y., Andreas, L., Griffin, R.G., 2015. Magic angle spinning NMR of proteins: high-frequency dynamic nuclear polarization and (1)H detection. Annu. Rev. Biochem. 84, 465-497.

Thankamony, A. S. L.; Wittmann, J. J.; Kaushik, M.; Corzilius, B. 2017. Dynamic nuclear polarization for sensitivity enhancement in modern solid-state NMR. Prog. Nucl. Magn. Reson. Spectrosc., 102-103, 120–195.

Uluca, B., Viennet, T., Petrović, D., Shaykhalishahi, H., Weirich, F., Gönülalan, A., Strodel, B., Etzkorn, M., Hoyer, W., Heise, H., 2018. DNP-Enhanced MAS NMR: a Tool to Snapshot Conformational Ensembles of a-Synuclein in Different States. Biophys J., *114*, 1614–1623.

van der Cruijsen, E.A., Koers, E.J., Sauvee, C., Hulse, R.E., Weingarth, M., Ouari, O., Perozo, E., Tordo, P., Baldus, M., 2015. Biomolecular DNP-Supported NMR Spectroscopy using Site-Directed Spin Labeling. Chemistry 21, 12971-12977.

van der Wel, P.C., Hu, K.N., Lewandowski, J., Griffin, R.G., 2006. Dynamic nuclear polarization of amyloidogenic peptide nanocrystals: GNNQQNY, a core segment of the yeast prion protein Sup35p. J. Am. Chem. Soc. 128, 10840-10846.

Viennet, T., Viegas, A., Kuepper, A., Arens, S., Gelev, V., Petrov, O., Grossmann, T.N., Heise, H., Etzkorn, M., 2016. Selective Protein Hyperpolarization in Cell Lysates Using Targeted Dynamic Nuclear Polarization. Angew. Chem. Int. Ed. Engl. 55, 10746-10750.

Vitzthum, V., Borcard, F., Jannin, S., Morin, M., Mieville, P., Caporini, M.A., Sienkiewicz, A., Gerber-Lemaire, S., Bodenhausen, G., 2011. Fractional spin-labeling of polymers for enhancing NMR sensitivity by solvent-free dynamic nuclear polarization. Chemphyschem 12, 2929-2932.

Voinov, M.A., Good, D.B., Ward, M.E., Milikisiyants, S., Marek, A., Caporini, M.A., Rosay, M., Munro, R.A., Ljumovic, M., Brown, L.S., Ladizhansky, V., Smirnov, A.I., 2015. Cysteine-Specific Labeling of Proteins with a Nitroxide Biradical for Dynamic Nuclear Polarization NMR. J. Phys. Chem. B 119, 10180-10190.

Wylie, B.J., Dzikovski, B.G., Pawsey, S., Caporini, M., Rosay, M., Freed, J.H., McDermott, A.E., 2015. Dynamic nuclear polarization of membrane proteins: covalently bound spin-labels at protein-protein interfaces. J. Biomol. NMR 61, 361-367.